Available online at www.sciencedirect.com
ScienceDirect
Aerosol Science 38 (2007) 377–397
Journal of Aerosol Science
www.elsevier.com/locate/jaerosci

Particle deposition in turbulent duct flows—comparisons of different model predictions

Lin Tian, Goodarz Ahmadi*

Department of Mechanical and Aeronautical Engineering, Clarkson University, Potsdam, NY 13699-5725, USA

Received 24 October 2006; received in revised form 11 December 2006; accepted 19 December 2006

Abstract

Numerical studies of transport and deposition of nano- and micro-particles in turbulence flow field have been studied in the past few decades. In most current industrial applications, Reynolds averaged turbulence models were used due to its relative simplicity and computational efficiency. In this work, a series of numerical simulations were conducted to study the transport and deposition of nano- and micro-particles in a turbulent duct flow using different turbulence models. Commercial software (FLUENT^{TM} 6.1.22) was used for turbulence mean flow simulation. Simulations of the instantaneous turbulence fluctuation with and without turbulence near wall correction, and particle trajectory analysis were performed with the in-house PARTICLE (object-oriented C++) code, as well as with FLUENT^{TM} code with and the use of user's defined subroutines. The simulation results for different cases were compared with the available experimental data, and the accuracy of various approaches was evaluated. In addition, the importance of turbulence model, boundary conditions, and turbulence fluctuation particularly near wall on particle transport and deposition were carefully evaluated. It was shown that when sufficient care was given to the modeling effort, the particle deposition rates could be predicted with reasonable accuracy. The presented results could provide guidelines for selecting appropriate procedure for simulating nano- and micro-particle transport and deposition in various applications.

Keywords: Particle deposition; Nano-particles; Turbulent flow; Model comparison

1. Introduction

Micro- and nano-particle dispersion and deposition in turbulent flow field have attracted attention of many researchers in the past few decades due to its wide applications in xerography, micro-contamination control, chemical industries and air pollution controls. New emerging applications include developing efficient inhalation drug delivery devices, estimating personal exposure to particulate matters in indoor and outdoor environments, occurrence of asthma related to environmental particulate pollutants, and other bio-medical devices. To provide a reliable computational model to be used as a predictive tool for these advance applications, the characteristics of the continuous fluid phase and the discrete particle phase have to be resolved. In particular, the interactions between the micro- and nano-particle motions and turbulence eddies need to be properly accounted for. However, due to the complexity of turbulence itself, there is no completely satisfactory model for describing the gas–solid interaction in the finest scale that can be applied universally.

* Corresponding author.
E-mail address: ahmadi@clarkson.edu (G. Ahmadi).

0021-8502/$ - see front matter © 2007 Elsevier Ltd. All rights reserved.
doi:10.1016/j.jaerosci.2006.12.003

Nomenclature

C_0	particle mass concentration
C_c	Stokes–Cunningham slip correction factor
C_D	particle drag coefficient
d	particle diameter
d_{ij}	deformation rate tensor of the fluid
D	particle mass diffusivity
F_i^L	lift force
g_i	acceleration of gravity
g_i^+	nondimensional acceleration of gravity
G_i	Gaussian random number with zero mean and unit variance
k	turbulence kinetic energy
k^+	nondimensional surface roughness
K^+	nondimensional turbulence kinetic energy
K_b	Boltzmann constant
J	particle mass flux to the wall per unit time
l_ε	turbulence dissipation length scale in "two-layer zonal model"
l_μ	turbulence viscous length scale in "two-layer zonal model"
L_e	eddy length scale
n_i	Brownian force vector
N_0	initial number of particles
N_d	number of deposited particles
R_y	turbulence Reynolds number in "two-layer zonal model"
R_{ij}	Reynolds stress tensor of the fluid
Re_p	particle Reynolds number
S_0	spectral density of Gaussian
S	particle-to-fluid density ratio
Sc	Schmidt number
t	time
t_{cross}	particle eddy crossing time
t_d^+	non-dimensional time duration
T_L	particle Lagrangian integral time scale
T	absolute temperature
$\bar{u}_i, u_i, u_i'$	mean, instantaneous and fluctuation velocity vector of the fluid
U_{mean}	averaged stream-wise velocity of the channel cross section
u^*	shear velocity of the fluid
u_i^p	velocity vector of particle
u^{+*}	nondimensional mean stream-wise velocity in standard wall function
U^+	nondimensional mean stream-wise velocity
$\underline{u}_d^+$	Particle nondimensional deposition velocity
v^+	nondimensional turbulence normal fluctuation velocity
x_i	position vector, $i = 1, 2, 3$ for stream-wise, lateral and span-wise direction
y^+	nondimensional wall unit
y^{+*}	nondimensional wall unit in standard wall function
ρ	mass density of the fluid
ν	kinematic viscosity of the fluid
ν_T	eddy viscosity of the fluid
τ_w	wall shear stress of the fluid
ε	turbulence dissipation rate
τ_e	eddy lift time

τ	particle relaxation time
λ	gas molecular mean free path
τ^+	nondimensional particle relaxation time
ζ	uniformly distributed random number between zero and one
ξ_i	Gaussian white-noise random number

Currently, there are three general approaches for simulating turbulent fluid flows. These are: Reynolds-averaged Navier–Stokes (RANS) equation method, direct numerical simulation (DNS), and large eddy simulation (LES). While DNS provides the most promising capability to reproduce features of turbulence up to the smallest Kolmogorov scale, the computational expenses associated with current algorithm and computing resources make it inapplicable for large *Re* or complex geometry applications. In the LES approach the large eddies are directly simulated, while eddies smaller than the grid scales are modeled. LES is expected to provide a better representation of turbulence features beyond the filtered scales; however, the needed computational resources are still extensive. While the limitations of DNS and LES stated here make them impractical for applications to complex regions of industrial interest, these approaches have greater potential with advances with development of efficient algorithms and/or availability of ever increasing computing resources. For current industrial applications of flows with large Re in complex passages, RANS remains as the most commonly used approach.

Extensive reviews of theoretical and experimental studies of behavior of particles in turbulent flows were provided by Wood (1981), Hinds (1984), Hidy (1984) and Papavergos and Hedley (1984). Computer simulation models for analyzing particle transport, deposition in turbulent flow field were reported by many researchers. Ounis and Ahmadi (1990) conducted analysis of dispersion of small spherical particles in random turbulent flow field with energy spectral method. Li and Ahmadi (1992, 1993, 1995) and He and Ahmadi (1999) developed computer simulation procedures for studying particle dispersion and deposition in various passages. In these earlier works, the flow field was simulated using empirical expressions, thermodynamically consistent rate-dependent turbulence model, and upgraded stress transport models. Fan and Ahmadi (1993) proposed a sub-layer model to capture the effect of near-wall vortical structure of turbulent on particle deposition in vertical ducts.

Matida, Nishino, and Torii (2000) reported statistical simulation of particle deposition from turbulent dispersed pipe flow with mean turbulence profile obtained from fitted DNS data. Wang and James (1999) proposed an anisotropic correction to isotropic turbulence models to study turbulent dispersion and deposition of small particles. McLaughlin (1989), Ounis, Ahmadi, and McLaughlin (1993), Zhang and Ahmadi (2000) conducted particle deposition in turbulent duct flows using the direct numerical simulation technique. Wang and Squires (1996) reported LES of particle-laden turbulent channel flow. Uijttewaal and Oliemans (1996) reported the study of particle dispersion and deposition in vertical pipe flows with both DNS and LES simulations. Kvasnak, Ahmadi, and Schmidt (2004) employed a Langevin model for simulating the turbulence fluctuation in connection with their study of spray droplets formation in turbulent flows. Oesterle and Zaichik (2004) studied the effect of Lagrangian time scales on particle dispersion modeling in equilibrium turbulent shear flows.

More recently, researches have been conducted to simulate nano- and micro-scale particle depositions in complex geometries. Examples of such studies for human lung were reported by Martonen, Zhang, and Yang (1992), Balashazy and Hofmann (1995), Li and Ahmadi (1995), and Zhang and Kleinstreuer (2001). Modeling of indoor particle depositions from turbulent flows were reported by Lai and Nazaroff (2000), among others. In these studies, RANS with k–ε, k–ω, and Reynolds stress transport model (RSM) were mostly used. The capability to capture the effect of turbulence fluctuation velocity field on particle has been the key in success or failure of these approaches.

In this study, simulations of nano- and micro-particle depositions in turbulent duct flows were conducted. Two RANS models, namely, the two-equation k–ε model and the RSM were used. Turbulent mean flows were simulated with the commercial software package (FLUENT^{TM} 6.1.22). Simulations of turbulence fluctuation including the near-wall correction, and particle trajectory analysis were conducted using the in-house PARTICLE (Object-oriented C++) code. In addition, the simulations were repeated using FLUENT^{TM} 6.1.22 discrete phase module (DPM) for comparison. One goal of the study has been to assess the effectiveness of RANS method with various modeling elements on the accuracy of predicted particle deposition rate in turbulent duct flows. The other object has been to test the performance of FLUENT^{TM} 6.1.22 for particle transport and deposition studies.

Results of the present simulations were compared with the available experimental data, empirical equations, and earlier simulation results. It was shown that the use of an appropriate anisotropic turbulence model was important for accurate predictions of the nano- and micro-particle transport in turbulent flow fields. The corresponding particle deposition rates were found to be sensitive to the near-wall correction used in the simulation. That is, in addition to the proper boundary condition for the mean flow velocity, the correct estimate of the turbulence near-wall fluctuation was important for accurate simulation of particle deposition rate.

The present work provides the first detailed comparative study of accuracy of various turbulence models for particle transport and deposition in duct flows. In particular, the importance of the effect of near-wall turbulence fluctuation was made clear. The duct flow was studied in detail for which a lot of experimental data and empirical equations are available that could be used for assessing the accuracy of different approaches. The finding, however, could provide guidelines for selecting appropriate procedure for simulating nano- and micro-particle transport and deposition in complex passages.

2. Turbulent flow field simulation

2.1. Mean flow field

The mean velocity field is evaluated by solving the RANS and continuity equation (White, 2006). The corresponding Reynolds stress tensor, $R_{ij} = \overline{u_i' u_j'}$ (where u_i' is the fluctuation velocity), was evaluated using the standard k–ε model that uses the Boussinesq eddy viscosity hypothesis. That requires two additional transport equations for turbulence kinetic energy k and turbulence dissipation ε. Another approach is to include the transport equation for the Reynolds stress tensor, R_{ij}, which eliminates the need for an eddy viscosity assumption. One advantage of the RSM is that it accounts for the anisotropy of turbulence. The description of the k–ε model and the RSM may be found in the work of Launder and Spalding (1972), Launder, Reece, and Rodi (1975) and in FLUENT User's Guide (1998).

2.2. Turbulent fluctuations

In turbulent flow field, turbulence diffusion by instantaneous flow fluctuations is the main mechanism for particle dispersion and depositions. This is in addition to the other mechanisms such as molecular diffusion, convective transport and gravitational sedimentation. Therefore, it is critical to incorporate appropriate model for simulating turbulence fluctuations for accurate analysis of particle transport and deposition processes. The most faithful simulation of fluctuation velocity should be able to capture the details of the turbulence eddy structures. Currently, this is only possible by the DNS that is only practical for low Reynolds number duct flows. For practical applications, however, turbulence fluctuation is mainly estimated using a variety of stochastic approaches. To account for near-wall coherent eddies, Fan and Ahmadi (1993) proposed a sub-layer model using a plane stagnation point flow. For reproduction of fluctuation with stochastic method, Kvasnak et al. (2004) employed a pdf-based Langevin equation to generate the instantaneous velocity and velocity gradient fields. Oesterle and Zaichik (2004) used a new more detailed stochastic model for analyzing turbulence dispersion.

In this work, two stochastic models for simulating turbulence fluctuations were used. PARTICLE code uses the continuous filter white-noise (CFWN) model proposed by Thomson (1987). Discrete Random Walk Model (DRW), initiated by Hutchinson, Hewitt, and Dukler (1971) and extended by others, has been incorporated into FLUENT^{TM} DPM for particle dispersion study in turbulence flow field.

2.2.1. Continuous filter white-noise (CFWN) model

PARTICEL code implemented the stochastic CFWN model of Thomson (1987) for numerical simulation of turbulent fluctuations as encountered by the discrete phase particles. We followed the procedure suggested by He and Ahmadi (1999) with slight difference in turbulence length scale. In this model, the instantaneous fluid velocity is simulated for given the turbulence local mean velocity and mean square fluctuations via the following Langevin equation:

$$\frac{\mathrm{d}u_i}{\mathrm{d}t} = -\frac{u_i - \overline{u_i}}{T_L} + \left(\frac{2\overline{u_i'^2}}{T_L}\right)^{1/2} \xi_i(t). \tag{1}$$

Here T_L is the particle Lagrangian integral time scale, and $\xi_i(t)$ is a vector Gaussian white-noise random process with spectral density $1/\pi$. The particle Lagrangian integral time scale T_L in Eq. (1) is given as

$$T_L = \int_0^\infty \frac{\overline{u'_p(t)u'_p(t+s)}}{u'_p(t)^2}\,ds. \tag{2}$$

For small particles that follow the flow, a good approximation for T_L is the local turbulence Lagrangian time scale. Proper estimate of T_L were discussed in a number of papers in the literature. Empirical eddy scales from pipe flow were used by Hutchinson et al. (1971), and Schuen, Chen, and Faeth (1983) suggested using the isotropic turbulence eddy scales from the k–ε model. Kallio and Reeks (1989) estimated T_L using an isotropic expression related to turbulence kinetic energy k and dissipation rate ε, and accounted for the near-wall in-homogeneity by introducing a randomized integral scale parameter. Graham and James (1996) proposed the use of $2T_L$ for more consistent model comparisons with the experimental data. Most expressions used for T_L in the past are given as

$$T_L = C_1\frac{k}{\varepsilon}. \tag{3}$$

Here, C_1 is the model constant. No universal value for C_1 has been found as yet; however, typically a value of C_1 in the range of 0.2 to 0.96 have been reported in literature for producing satisfactory results for comparison with the experimental data. Eq. (3) originated from isotropic turbulent flow fields; for inhomogeneous and anisotropic flows, the value of T_L may be estimated with the modified version of the equation using the lateral turbulence mean square fluctuations. That is,

$$T_L = C_2\frac{\overline{u'_2u'_2}}{\varepsilon}, \tag{4}$$

where constant C_2 is of the same order as C_1. Matida et al. (2000) suggested $C_2 = 1.0$. Recently, a more detailed modeling procedure for estimating the Lagrangian time scales in turbulent shear flows was reported by Oesterle and Zaichik (2004) where a Lagrangian equation was used.

In this work, Eq. (3) was used for evaluating the turbulence Lagrangian time-scale for simulation with the k–ε model. Eq. (4) was implemented into PARTICLE code for use with the anisotropic RSM turbulence model.

During the simulation of Eq. (1), at every time step the amplitude of the white noise process, $\xi_i(t)$, is evaluated as

$$\xi_i(t) = \frac{G_i}{\sqrt{\Delta t}}, \tag{5}$$

where G_i is selected from a population of independent Gaussian random numbers with zero mean and unit variance. The entire white noise sample is then shifted by $\Delta t\zeta$ where ζ is a uniform random number in the range of (0,1).

2.2.2. Discrete random walk (DRW) model

The "Eddy Lifetime" model is used for the stochastic tracking in the FLUENT^{TM} code. This model assumes successive encounter of particles with discrete turbulence eddies. In this model, fluctuation velocity is given as

$$u'_i = G\sqrt{\overline{u'^2_i}}, \tag{6}$$

where G is a zero mean, unit variance normally distributed random number, $\sqrt{\overline{u'^2_i}}$ is the root mean-square (RMS) local fluctuation velocity in the ith direction. The RMS fluctuation velocities are directly evaluated in the RSTM model. For the k–ε model, the three components are assumed to be equal and are given as $\overline{u'^2_1} = \overline{u'^2_2} = \overline{u'^2_3} = \frac{2}{3}k$.

The time scale τ_e associated with each eddy (eddy life time) is given as

$$\tau_e = 2T_L, \tag{7}$$

where T_L is given by Eq. (3). In addition to the eddy lifetime, τ_e, a particle eddy crossing time t_{cross} is defined as

$$t_{cross} = -\tau\ln\left[1 - \left(\frac{L_e}{\tau|u - u_p|}\right)\right]. \tag{8}$$

Here τ is the particle relaxation time defined as

$$\tau = \frac{Sd^2 C_c}{18\nu}, \tag{9}$$

where S is the particle-to-fluid density ratio, d is the particle diameter, ν is the fluid kinematic viscosity, and C_c is the Stokes–Cunningham slip correction factor, which is given as

$$C_c = 1 + \frac{2\lambda}{d}(1.257 + 0.4e^{-(1.1d/2\lambda)}), \tag{10}$$

where λ is the gas molecular mean free path.

In Eq. (8), L_e is the eddy length scale, and $|\mathbf{u} - \mathbf{u}_p|$ is the magnitude of the relative slip velocity. The frequency of the particle encountering turbulence eddies is the reciprocal of the lesser of τ_e and t_{cross}.

In addition to evaluating τ_e with a constant T_L as expressed by Eq. (7), FLUENT^{TM} provide an alternative way for computing τ_e with a randomized T_L. That is,

$$\tau_e = -T_L \log(\zeta), \tag{11}$$

where ζ is a uniformly distributed random number between 0 and 1. Simulations in this study did not show an improvement with use of Eq. (11) for the eddy life time instead of Eq. (7), but with additional computing overhead. Therefore, Eq. (7) was used for all the subsequent simulations.

In this study, CFWN model that was implemented in PARTICLE code, also provided the flexibility for using Eqs. (3) or (4) for T_L. FLUENT^{TM} code, however, has a built-in DPM module, and used Eq. (3) for calculating T_L for the particle dispersion with the stochastic DRW model.

2.3. Turbulent near-wall model

For the study of nano- and micro-scale particle depositions in wall-bounded turbulent flows, proper modeling of the near-wall region is crucial to the accuracy of the simulation results. The RANS k–ε and RSM models were formulated primarily for turbulent flows in the core region; therefore, some improvements in the near-wall region are needed for more realistic simulations. Following sections cover the near-wall treatments in the current simulation study, and how they are incorporated into the PARTICLE and FLUENT^{TM} codes.

2.3.1. Standard wall function boundary condition

Standard wall function is the most commonly used boundary condition for turbulent flows in industry applications. Accordingly, the "law of the wall" for turbulent stream-wise mean velocity profile is imposed at the adjacent grid points from the wall. That is,

$$u^{+*} = y^{+*} \quad \text{for } y^{+*} < 11.225, \tag{12}$$

$$u^{+*} = \frac{1}{\kappa}\ln(Ey^{+*}) \quad \text{for } y^{+*} > 11.225, \tag{13}$$

where "$+*$" denotes the wall units and the nondimensional velocity and distance from the wall are given as

$$u^{+*} \equiv \frac{uc_\mu^{1/4}k^{1/2}}{\tau_w/\rho}, \quad y^{+*} \equiv \frac{\rho c_\mu^{1/4}k^{1/2}y}{\mu}, \tag{14}$$

with $\kappa = 0.42$, $E = 9.81$.

With the standard wall function boundary condition, turbulence variables for cells adjacent to the wall are obtained through semi-empirical equations based on local turbulence equilibrium assumption. Accordingly, the expression for turbulence kinetic energy k and dissipation rate ε are given as

$$k = \frac{\tau_w}{\rho\sqrt{c_\mu}}, \tag{15}$$

$$\varepsilon = \frac{c_\mu^{3/4} k^{3/2}}{\kappa y}. \tag{16}$$

Away from the wall where turbulence is in the fully developed regime, turbulence kinetic energy and dissipation rate are computed through the corresponding transport equations.

The standard wall function boundary condition is most frequently used in practical applications because of its ease of use, computational efficiency, and stability. It, however, is known that the standard wall function does not account for many of the complexities of turbulence near wall flows. In this study, the accuracy of the use of the standard wall function boundary condition in connection with deposition of nano- and micro-scale particles is evaluated. A series of computer simulations are conducted with both PARTICLE and FLUENT^{TM} codes. As noted before, the standard wall function is the default boundary condition for the k–ε and RSM models in FLUENT^{TM} code. It is found that the use of the standard wall function boundary condition may lead to inaccurate estimate of particle deposition rates.

2.3.2. Two-layer zonal model

Chen and Patel (1988) proposed a two-layer wall boundary condition for resolving the near-wall features of the flow. The model makes use of Wolfshtein's (1969) one-equation model to account for the near-wall effect. Beyond the "Buffer Layer" and part of the log layer, the traditional RANS turbulence models are used. In the near-wall layer, turbulence kinetic energy k is evaluated through its transport equation, while the dissipation rate ε and eddy viscosity ν_t are estimated as,

$$\varepsilon = \frac{k^{3/2}}{l_\varepsilon}, \tag{17}$$

$$\nu_t = C_\mu \sqrt{k} l_\mu. \tag{18}$$

In Eqs. (17) and (18), the wall effects are taken into account with damping of the length scales l_ε and l_μ with the following characteristics:

$$l_\mu = C_1 y(1 - \mathrm{e}^{-(R_y/A_\mu)}), \tag{19}$$

$$l_\varepsilon = C_1 y(1 - \mathrm{e}^{-(R_y/A_\varepsilon)}). \tag{20}$$

Here the constants are: $C_1 = \kappa C_\mu^{3/4}$, $A_\mu = 70$, $A_\varepsilon = 2C_1$. In Eqs. (19) and (20), R_y is the turbulence Reynolds number defined in near-wall region as

$$R_y = \frac{y\sqrt{k}}{\nu}. \tag{21}$$

The damping of turbulence imposed by Eqs. (19) and (20) reaches the maximum at wall, and it decays with distance further away from the wall. The transition from the near-wall layer to the core region is made when R_y reaches 200.

Two-layer zonal near-wall model provides a simple way for accounting for the near-wall effects on turbulence features. The two-layer wall boundary condition is provided as an option in FLUENT^{TM} code version 6.1.22. Accordingly, having the first grid point at $y^+ = 1$ is recommended for an accurate simulation. The two-layer wall boundary condition was also used in this study as one of the test cases.

2.3.3. Quadratic variation near wall

It is well known that continuity requires the RMS turbulence fluctuation normal to wall to follow a quadratic variation (Hinze, 1975). Experiment measurements as well as DNS simulations of Kim, Moin, and Moser (1987) and Ounis et al. (1993) have verified this trend of variation. Accordingly,

$$\sqrt{\overline{v'^2}} \propto y^2 \quad \text{as } y \to 0. \tag{22}$$

$$v^{+\prime} = A y^{+2} \quad \text{for } y^+ < 4, \tag{23}$$

where $y^+ = yu^*/\nu$ and $v^{+\prime} = \sqrt{\overline{v'^2}}/u^*$. Here the shear velocity is defined as $u^* = \sqrt{\tau_w/\rho}$, and τ_w is the wall shear stress.

Using the DNS analysis of near-wall flows, Ounis et al. (1993) suggested, $A = 0.008$, which was also in agreement with the work of Kim et al. (1987). Li and Ahmadi (1992, 1993) corrected for the quadratic variation of the normal fluctuation velocity in their study of particle depositions in turbulent flows and noted its profound effects. Accordingly, proper estimate of $v^{+\prime}$ significantly affects the particle deposition rate on the wall. This correction can be conveniently added to any computational model for improving the accuracy of the particle deposition rate. In this study, the "quadratic variation" is implemented in PARTICLE code.

3. Particle equation of motion

In this study, it is assumed that flow is sufficiently dilute and that the airflow field is not affected by the presence of particles. The governing equation of motion is given as

$$\frac{\mathrm{d}u_i^{\mathrm{p}}}{\mathrm{d}t} = \frac{1}{\tau}\frac{C_{\mathrm{D}}Re_{\mathrm{p}}}{24}(u_i - u_i^{\mathrm{p}}) + F_i^{\mathrm{L}} + g_i + n_i(t). \tag{24}$$

Here $u_i^{\mathrm{p}} = \mathrm{d}x_i/\mathrm{d}t$ is the particle velocity, F_i^{L} is the lift force, g_i is acceleration of gravity, $n_i(t)$ is the Brownian force per unit mass, and τ is the particle relaxation time given by Eq. (9). In Eq. (24) C_{D} is the drag coefficient (Hinds, 1984), which is defined as

$$C_{\mathrm{D}} = \frac{24}{Re_{\mathrm{p}}} \quad \text{for } Re_{\mathrm{p}} < 1, \tag{25}$$

and

$$C_{\mathrm{D}} = \frac{24}{Re_{\mathrm{p}}}(1 + 0.15Re_{\mathrm{p}}^{0.687}) \quad \text{for } 1 < Re_{\mathrm{p}} < 400. \tag{26}$$

Here Re_{p} is the particle Reynolds number, and is defined as

$$Re_{\mathrm{p}} = \frac{\mathrm{d}|u_j - u_j^{\mathrm{p}}|}{v}. \tag{27}$$

The lifting force in Eq. (24) is given as

$$F_i^{\mathrm{L}} = \frac{2Kv^{1/2}d_{ij}}{Sd(d_{lk}d_{kl})^{1/4}}(u_j - u_j^{\mathrm{p}}), \tag{28}$$

where $K = 2.594$ is the constant coefficient of Saffman lift force (Saffman, 1965), and d_{ij} is the deformation rate tensor given as

$$d_{ij} = \frac{1}{2}\left(\frac{\partial u_i}{\partial x_j} + \frac{\partial u_j}{\partial x_i}\right). \tag{29}$$

The Brownian excitation, $n_i(t)$, is modeled as a Gaussian white noise random process with a spectral density S_0 given as (Li & Ahmadi, 1992)

$$S_0 = \frac{216vk_{\mathrm{b}}T}{\pi^2\rho d^5 S^2 C_{\mathrm{c}}}. \tag{30}$$

Here, $k_{\mathrm{b}} = 1.38 \times 10^{-23}$ J/K is the Boltzmann constant, T is the absolute temperature, ρ is the fluid density.

Eq. (24) for particle trajectory analysis includes the effect of hydrodynamic drag force introduced by relative slip velocity, the Saffman lift force due to shear in the flow field, Brownian excitation due to molecular impact, and the gravitational force. In Eq. (24), the effect of turbulence on transport and dispersion of particles is introduced through the instantaneous velocity, $u_i = \overline{u_i} + u_i'$.

4. Deposition velocity and empirical models

The simulation result for particle deposition is commonly presented in the form of nondimensional deposition velocity for comparison with the experimental data and empirical models. The nondimensional deposition velocity for particles released with uniform concentration C_0 near a surface is given by

$$u_{\mathrm{d}}^{+} = \frac{J}{C_0 u^*}, \tag{31}$$

where J is the particle mass flux to the wall per unit time and u^* is the flow shear velocity. The nondimensional particle relaxation time is defined as

$$\tau^{+} = \frac{\tau u^{*^2}}{\nu} = \frac{Sd^2 u^{*^2}}{18\nu^2} C_{\mathrm{c}}. \tag{32}$$

In the computer simulation, the particle deposition velocity can be estimated as

$$u_{\mathrm{d}}^{+} = \frac{N_{\mathrm{d}}/t_{\mathrm{d}}^{+}}{N_0/y_0^{+}}, \tag{33}$$

where N_0 is the initial number of particles uniformly distributed in a region within a distance of y_0^{+} from the wall, and N_{d} is the number of deposited particles in the time duration t_{d}^{+}. Here, $y_0^{+} = y_0 u^*/\nu$ and $t_d^{+} = t_d u^{*^2}/\nu$, where y_0 and t_{d} are corresponding dimensional values used in the computer simulation.

In this study, in addition to comparison with experimental data, the numerical simulation results are compared with the semi-empirical model predictions. A simple empirical equation for the nondimensional deposition velocity suggested by Wood (1981) is given as

$$u_{\mathrm{d}}^{+} = 0.057 S_c^{-2/3} + 4.5 \times 10^{-4} \tau^{+^2} + u_t^{+}, \tag{34}$$

where $S_c = \nu/D$ is the Schmidt number with D being the particle mass diffusivity given as

$$D = \frac{K_{\mathrm{b}} T}{3\pi\mu d} C_c. \tag{35}$$

In Eq. (34), the last term accounts for the contribution to particle deposition velocity by gravitational sedimentation in horizontal duct, which is defined as

$$u_t^{+} = \tau^{+} g^{+}, \tag{36}$$

where g^{+} is expressed with the following form:

$$g^{+} = \frac{\nu}{u^{*3}} g. \tag{37}$$

Fan and Ahmadi (1993) developed an empirical equation for deposition of particles in vertical ducts including the effects of surface roughness and gravity along the flow direction which is given as

$$u_d^{+} = \begin{cases} 0.084 S_c^{-2/3} + \dfrac{1}{2}\left[\dfrac{(0.64k^{+} + \frac{1}{2}d^{+})^2 + \dfrac{\tau^{+^2} g^{+} L_1^{+}}{0.01085(1+\tau^{+^2} L_1^{+})}}{3.42 + (\tau^{+^2} g^{+} L_1^{+})/(0.01085(1+\tau^{+^2} L_1^{+}))}\right]^{1/(1+\tau^{+^2} L_1^{+})} \\ \quad \times [1 + 8\mathrm{e}^{-(\tau^{+}-10)^2/32}] \dfrac{0.037}{1 - \tau^{+^2} L_1^{+}(1 + (g^{+}/0.037))} & \text{if } u_{\mathrm{d}}^{+} < 0.14 \\ 0.14 & \text{otherwise.} \end{cases} \tag{38}$$

Here, $L_1^{+} = 3.08/(Sd^{+})$, $g^{+} = \nu/u^{*^3} g$, and k^{+} is the surface roughness (which is set to zero for smooth surface in this study). For a horizontal channel, $g^{+} = 0$ in Eq. (38) and the gravitational sedimentation velocity $\tau^{+} g^{+}$ must be added to this expression.

5. Results and discussions

5.1. Computational domain

In this study, the flow in a 0.02 m wide, 0.4 m long two-dimensional duct is studied. A structured grid with 0.5 mm cell dimension in both stream-wise and lateral directions was generated for the duct core region. Near the wall boundaries, a higher mesh resolution in lateral direction was generated with first grid point located at 0.05 mm away from the wall that evolves to the core region with a growing factor of 1.2 in normal direction. Gambit code was used for the mesh generation and a total of 44,000 quadrilateral elements were created in the computational domain.

For the core region, the 0.5 mm cell dimension was shown to be sufficient by comparing the simulation result with a refined grid of 0.25 mm cell dimension. Mesh independency check was conducted in more detail in the near-wall region where solutions are expected to be more sensitive to grid size. A coarse near boundary mesh resolution with first grid point located at 0.1 mm, and finer boundary meshes with first grid point located at 0.01, 0.005, 0.001 and 0.0005 mm were tested. The study showed grid consistency for the flow conditions was reached for the first grid point being at 0.05 mm. For particle deposition, however, grid sensitivity was generally observed. The level of grid dependency was also affected by the use of different modeling techniques for the generation of turbulence fluctuations and turbulent wall boundary condition. With inclusion of "quadratic variation of normal fluctuation velocity near the wall," however, the simulations reached grid consistency even with the coarser mesh. In absence near wall correction, however, the simulation results for particle deposition for both "standard wall function boundary condition" and "two-layer near wall model" were found to be affected by the grid resolution up to the finest level considered. With the standard wall function, no satisfactory particle deposition results were obtained with all mesh resolutions considered. Optimal results were obtained with "two-layer zonal wall boundary condition" when the first grid point is located at about one wall unit as suggested by the model developers. Therefore, a mesh resolution with 0.5 mm cells in the core region together with a staggered boundary mesh with first grid point being at 0.05 mm, which was about 1.13 wall units, was considered for the present comparative studies. Fig. 1 shows the schematic discretization of the computational domain.

5.2. Flow field simulation

The air properties used in the simulations were: $T = 288\,\mathrm{K}$, dynamic viscosity $\mu = 1.84 \times 10^{-5}\,\mathrm{ns/m^2}$, and density $\rho = 1.225\,\mathrm{kg/m^3}$. A fully developed turbulence channel flow profile was imposed at the inlet with stream-wise turbulent

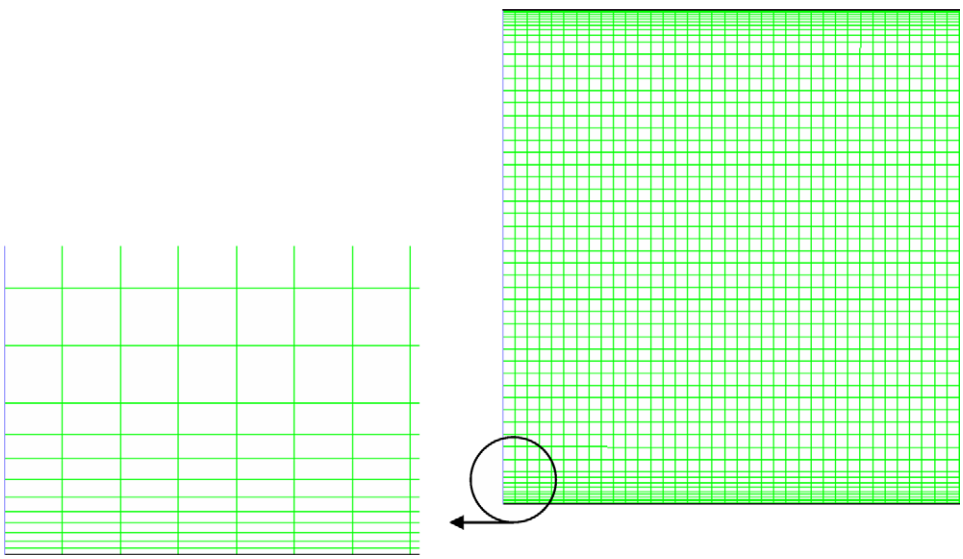

Fig. 1. Computational grid.

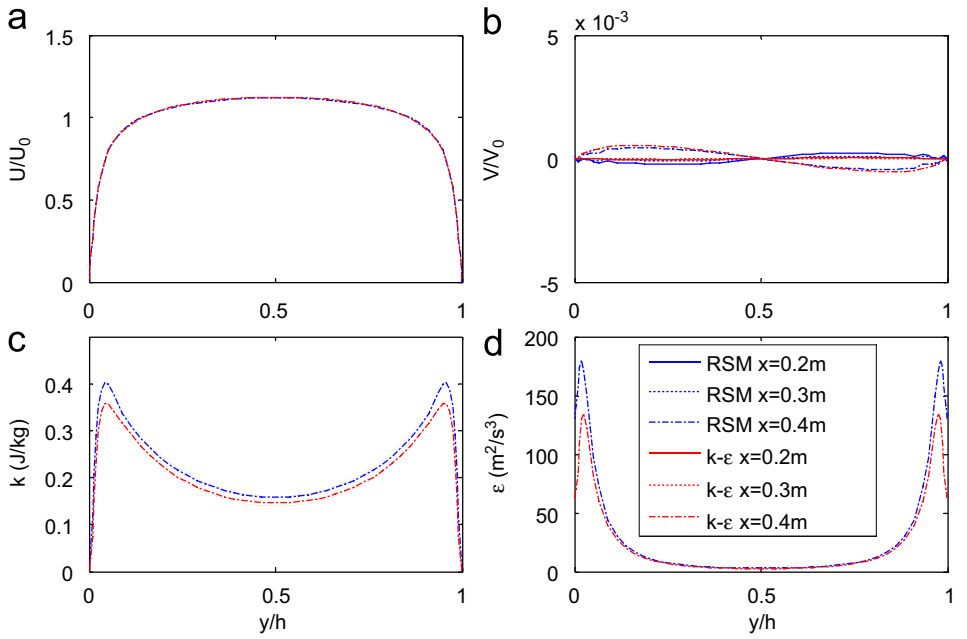

Fig. 2. Comparison of (a) mean axial velocity, (b) mean vertical velocity, (c) turbulence kinetic energy, and (d) turbulence dissipation rate profiles at three-channel cross sections as predicted by the RSM and the k–ε models with near wall "two-layer zonal" boundary condition.

mean velocity modeled with 1/7th power law given by,

$$U = \frac{8}{7}U_{\text{mean}}\left(\frac{y}{h/2}\right)^{1/7} \quad \text{for } 0 \leqslant y \leqslant \frac{h}{2}, \tag{39}$$

and

$$U = \frac{8}{7}U_{\text{mean}}\left(\frac{h-y}{h/2}\right)^{1/7} \quad \text{for } \frac{h}{2} < y \leqslant h. \tag{40}$$

Here, $h = 0.02$ m, is the channel width, $U_{\text{mean}} = 5.0$ m/s is the averaged velocity of the channel cross section. Turbulence kinetic energy k at inlet was assumed to vary linearly from the near-wall value given by Eq. (15), to the core region value with following expression:

$$k = \frac{\tau_{\text{w}}}{\rho\sqrt{c_\mu}} + \frac{y}{h/2}\{0.002[8U_{\text{mean}}/7]^2 - \frac{\tau_{\text{w}}}{\rho\sqrt{c_\mu}} \quad \text{for } 0 \leqslant y \leqslant \frac{h}{2}, \tag{41}$$

and

$$k = \frac{\tau_{\text{w}}}{\rho\sqrt{c_\mu}} + \frac{h-y}{h/2}\{0.002[8U_{\text{mean}}/7]^2 - \frac{\tau_{\text{w}}}{\rho\sqrt{c_\mu}} \quad \text{for } \frac{h}{2} < y \leqslant h. \tag{42}$$

Turbulent dissipation rate at inlet was evaluated by Eq. (16). The Reynolds number based on average velocity and channel width was 6667, which indicates a turbulent flow condition. The flow was driven by pressure gradient in stream-wise direction and standard no slip boundary condition was applied to the wall. Second-order upwind scheme was used for solving the momentum equation and additional transport equations associated with the RANS models.

Fig. 2 shows mean velocity and turbulence profiles at three cross sections along the second half of the duct. Results from the RSM and k–ε models with "two-layer zonal model" are presented. Data of all the relevant variables from three locations collapse into one single line indicating a fully developed turbulent state in the latter half of the channel. While the V-velocity component profiles across the three sections shown in Fig. 2b vary from each other,

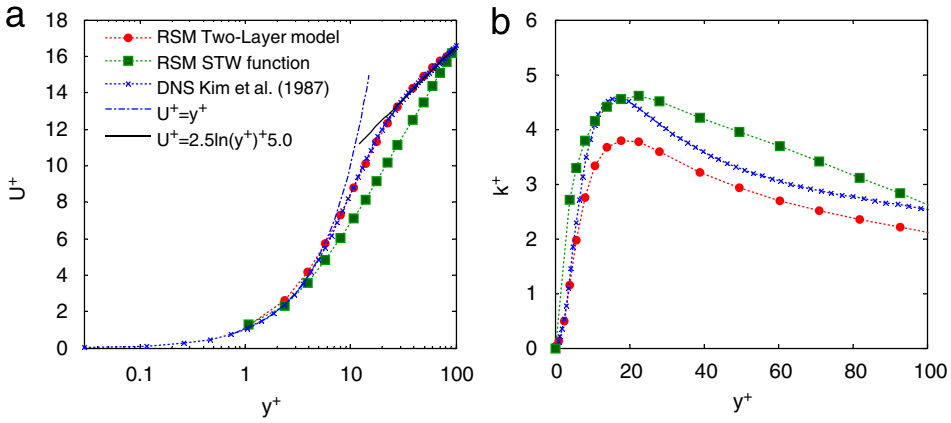

Fig. 3. Nondimensional stream-wise mean velocity and turbulence kinetic energy profiles in fully developed channel flows in wall units.

the scale is in the order of $10^{-4}U_0$; therefore, the flow is nearly in the fully developed regime. It is also observed from Fig. 2 that the mean flow simulation results obtained from the k–ε and the RSM models are quite similar when "two-layer zonal model" boundary conditions are used. While both models predicate the highest turbulence intensity occurring very close to the wall between 10 to 20 wall units, slightly higher turbulence intensity is predicated by the RSM model.

Mean velocity and turbulence profiles at the same three cross sections as in Fig. 2 but with the standard wall function boundary condition were also studied. However, the results are not shown here due to the space limitation. Examination of those results shows certain discrepancy of the model prediction with the trend of experimental data.

In particular, the predicted dissipation rate predicted with the use of the "standard wall function boundary condition" significantly overestimates the prediction of the "two-layer zonal model" and the experimental data.

Fig. 3 shows the stream-wise mean velocity and turbulence kinetic energy profiles in the near-wall region in the latter half of the channel. Here flow is nearly fully developed and the profiles are shown in wall units. Simulations from the RSM model with the "two-layer zonal model" and with the "standard wall function boundary conditions" are shown in this figure for comparison. DNS results from Kim et al. (1987) are also reproduced in this figure for comparison. For stream-wise mean velocity, the semi-empirical equations for the viscous sublayer and the "log law" regions as given by Eqs. (12) and (13) are plotted. Here $U^+ = u/u^*$ and $K^+ = k/u^{*2}$ are nondimensional velocity and turbulence kinetic energy. For the fully developed portion of the duct flow, $u^* = 0.342$ m/s. Fig. 3 shows that with the "two-layer zonal" boundary condition, the RSM model is able to reproduce the turbulence near-wall features that are in agreement with the DNS simulation. The predicted mean velocity profile is also in agreement with the empirical equations. For this high resolution grid, when the "standard wall function" is used, however, the RSM predication of U^+ deviates from the DNS and semi-empirical equations. In particular, k^+ is overpredicted for $y^+ < 5$.

When "two-layer zonal" boundary condition is used, Figs. 2 and 3 show that both the RSM and k–ε models lead to reasonable turbulence mean quantities. When the "standard wall function boundary condition" is used, the accuracy of the near-wall predictions of both RSM and k–ε models are degraded. The k–ε model with the standard wall function appears to lead to the least reliable predications.

Fig. 4 shows the nondimensional RMS turbulence velocity fluctuations in stream-wise, lateral and span-wise directions as predicted by the RSM and the k–ε models. Here the "two-layer zonal" boundary condition was used. The DNS predications of Kim et al. (1987) are also reproduced in this figure for comparison. As is expected, Fig. 4 shows that the turbulence fluctuating velocities are highly anisotropic in the near-wall region, but tend toward an isotropy near the channel centerline. Near the wall the stream-wise fluctuation has the highest magnitude and the lateral fluctuation has the lowest, and these variations are well captured by the RSM model. The RSM model predictions for the turbulence fluctuation velocities are in reasonable agreement with the DNS simulation data. Due to the limitation of isotropic eddy viscosity assumption, the k–ε model cannot provide information concerning the near-wall anisotropy of turbulence.

Fig. 5 shows the variation of the nondimensional RMS lateral fluctuation velocity very close to the wall in the latter half of the channel as predicted by the RSM model with the "two-layer zonal" boundary condition. Simulation results

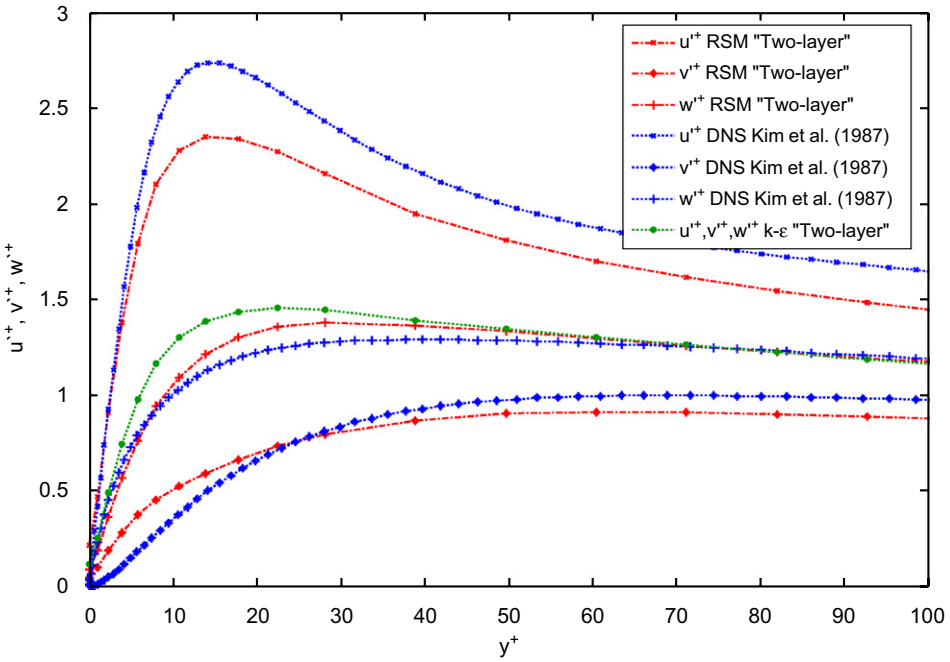

Fig. 4. Nondimensional root mean square turbulence velocity fluctuations in the fully developed channel flow.

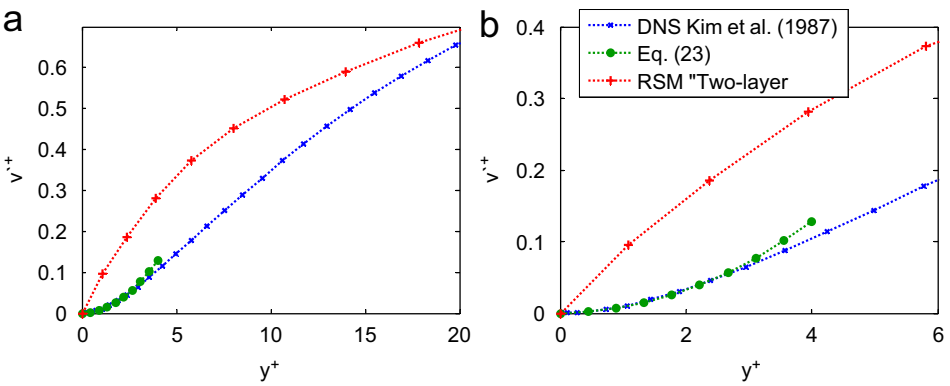

Fig. 5. Nondimensional root mean square lateral fluctuation velocity close to the wall in fully developed channel flow.

from the DNS of Kim et al. (1987), and the predication of Eq. (23) as suggested by Li and Ahmadi (1992, 1993) are also presented in this figure for comparison. The focus is within four wall units where both DNS simulation and model given by Eqs. (22) and (23) indicate a quadratic variation of lateral turbulence fluctuation. However, the profile predicated by the RSM model with the "two-layer zonal" boundary condition is higher than the DNS simulation. This discrepancy cannot be corrected by further refining the mesh. This is in part due to the fact that the "two-layer zonal" boundary condition is recommended to be applied at the grid point that is about one wall unit away from the wall. In addition, the linear interpolation of flow field variables between nodal points is the default algorithm in FLUENT^{TM} code. While the linear interpolation works fine for most quantities, the vertical fluctuation velocity vary with square of the distance from wall within four wall units distance as noted by Eqs. (22) and (23). Therefore, while the RSM model

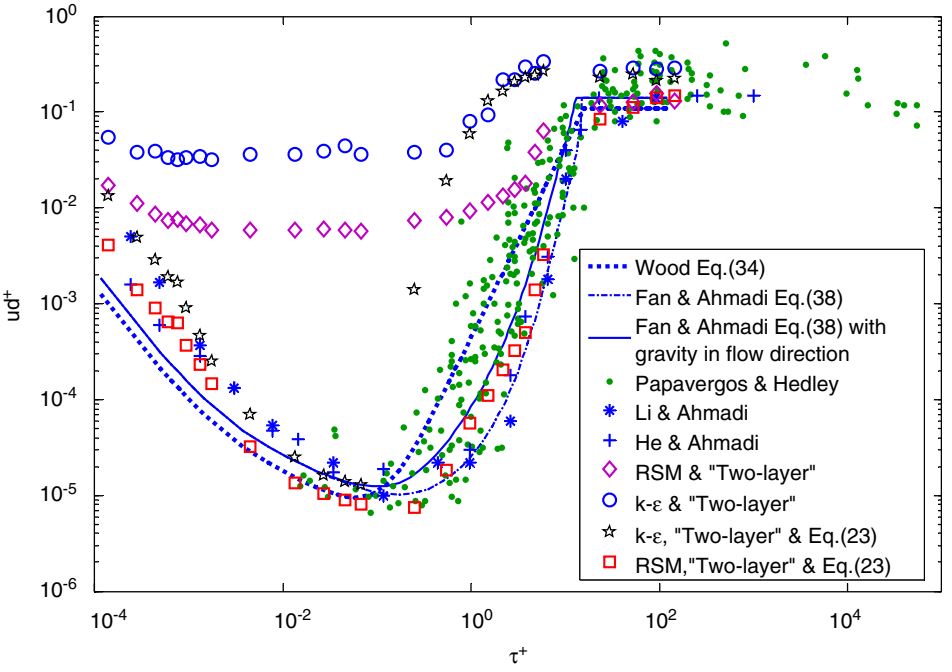

Fig. 6. Comparison of deposition velocity as predicted by the PARTICLE code (current simulation) and earlier results in a vertical duct with gravity in the flow direction.

with "two-layer zonal model" produces reasonable features of turbulence as shown in Fig. 4 and is considered superior to other RANS models, the linear nature of the interpolation scheme used at very short distance from the wall could still lead to high values of vertical fluctuations and consequently to higher particle deposition rates. This point will be further discussed in the subsequent sections.

5.3. *Particle simulation results*

Particle simulation results are presented in this section. In these simulations, particle sizes were varied from 0.01 μm (10 nm) to 50 μm, while the particle-to-fluid density ratio was kept fixed at $S = 2000$. Particle initial velocity was set equal to the local airflow velocity. The "trap" wall boundary condition for particle–wall interaction was used. This implies that particles will stick to the wall upon contact. Typically 3000 particles were released with a uniform distribution within the 30 wall units of the lower wall at the mid-section of the duct (at $x = 0.2$ m). Statistical consistency on the rate of deposition was reached even for lower ensemble populations in the Brownian and inertial dominated regions.

A series of computer simulations were performed and the accuracy of the particle deposition rates for different models including the two-equation k–ε model and the RSM was examined. The influence of the near-wall treatment of turbulence fluctuation perpendicular to the wall on particle deposition rate was studied. The limitation of different codes for predicating particle deposition in turbulent duct flows was examined.

Fig. 6 shows the variation of the simulated nondimensional particle deposition velocity, u_d^+, as a function of nondimensional particle relaxation time, τ^+ using different models and boundary conditions. Here, u_d^+ and τ^+ are, respectively, defined in Eqs. (31) and (32). The value of u_d^+ was evaluated with the use of Eq. (33) from the slope of the number of deposited particle with time. These particle trajectory simulations were performed with PARTICLE code that acts as a post processor to FLUENT code that generated the flow field. The experimental data of Papavergos and Hedley (1984), the empirical equations of Wood (1981), Fan and Ahmadi (1993), and the simulation results of Li and Ahmadi (1993), and He and Ahmadi (1999) are plotted in this figure for comparison. The simulations that are presented in Fig. 6 are

for the RSM and the k–ε turbulence model with the "two-layer zonal" boundary condition. For each case the effect of inclusion or omission of the near-wall normal fluctuation correction given by Eq. (23) are studied. The experimental data, the semi-empirical equations and simulation results presented in Fig. 6 show that the deposition velocities have a "V-shaped" variation for the particle in the size range of 0.01 to 50 μm. This range includes the "Brownian region" for ultra fine particles on the left side of the V-shaped curve and the inertial range on the right side. In the Brownian range, molecular diffusion is the dominant mechanism for particle deposition, and the deposition rate decreases with increasing particle size. The deposition velocity in "inertial region" corresponding to the turbulence inertial impaction regime, increases with increasing particle size, and reaches a constant value for very large particles. The "transition region" between the "Brownian" and "inertial" region lies in the valley of the V-shaped curve, where both the molecular diffusion and the inertial effects are small and the corresponding particle deposition rate reaches its minimum value. Fig. 6 shows that the RSM model with the "two-layer zonal" boundary condition and the near-wall "quadratic variations" correction leads to the deposition velocities that are closest to the experimental data and semi-empirical models predictions.

When the k–ε turbulence instead of the RANS model was used, under the same conditions, the corresponding deposition velocities are plotted with symbol "☆" in Fig. 6. While the predicted deposition velocity still exhibits a V-shaped curve, it deviated from the experimental data and the semi-empirical models. This is particularly evident for the larger particle sizes that the deposition velocity is overestimated. The simulation results indicate that even with careful inclusion of the near-wall corrections, the k–ε model cannot predict the particle deposition velocity in the "transition" and "inertial" regions.

Fig. 6 also shows the simulation results by the RSM and k–ε models without the near-wall correction for the turbulence normal fluctuation as given by Eq. (23). These simulation results for the RSM and k–ε models are, respectively, shown by "◇" and "o" in this figure. It is seen that omission of the quadratic variation of the turbulence fluctuation velocity leads to significant overestimation of the deposition velocity for almost the entire range of sizes studied. The amount of error for the k–ε model is higher than that for the RSM model due to the effect of turbulence anisotropy. Fig. 6 also shows that the V-shape variation of the deposition velocity curve is highly distorted and the range of "Brownian" and "transition" is hard to identify. This trend of behavior can be explained with the examination of Fig. 5 which shows higher values of turbulence normal fluctuation in the region within a few wall units. While this does not significantly affect the flow field, it affects the small particle deposition substantially.

In summary, Fig. 6 shows that the most accurate predication of particle depositions over the entire size range is achieved with the use of the RSM and the "two-layer zonal" boundary condition, and the inclusion of the near-wall correction as given by Eq. (23). The k–ε model that ignores turbulence anisotropy leads to overestimation of the particle deposition rate.

To study the effect of use of standard wall function boundary conditions on the deposition velocity a series of simulations identical to those presented in Fig. 6 were performed. Only here the standard wall function instead of "two layer zonal" boundary condition was used and the results are presented in Fig. 7. Particle code was then used to evaluate the particle trajectory and the corresponding deposition rates. It is seen that both the k–ε and the RSM model with the "standard wall function" significantly overpredicate the deposition velocities for particles over entire size range. The V-shape variation of the deposition velocity cannot be clearly observed for most cases in this figure. Comparing with Fig. 6, the overpredications are much higher than those of the k–ε and the RSM models with "two-layer zonal" boundary condition and with omission of the near-wall correction. Earlier discussion shows that the "standard wall function" boundary condition leads to turbulence intensities that are much higher than those of the experimental and the DNS predications. For both the RSM and the k–ε turbulence models together, when the normal fluctuation is corrected with the use of Eq. (23), the predicated u_{d}^{+} improves to an extent. The RSM model with the correction provided by Eq. (23) is able to provide reasonable results for the Brownian and the inertial region, but leads to overestimation in the "transition" region. Similar trend is observed for the k–ε model when the near-wall correction is included, however, with a larger error in the estimated deposition rate.

To study the accuracy of particle deposition rate as predicated by FLUENT$^{\mathrm{TM}}$ code, a series of simulations identical to those presented in Figs. 6 and 7 were performed. Here, however, the correction of near-wall normal turbulence fluctuation given by Eq. (23) could not be included due to the limitation of the unavailability of the source code. Fig. 8 compares the simulation results for the RSM and the k–ε turbulence models with the "two-layer zonal" boundary condition and the standard wall function boundary condition. It is seen that the RSM model with the "two-layer zonal" boundary condition leads to deposition velocities that are closest to the experimental data and semi-empirical model

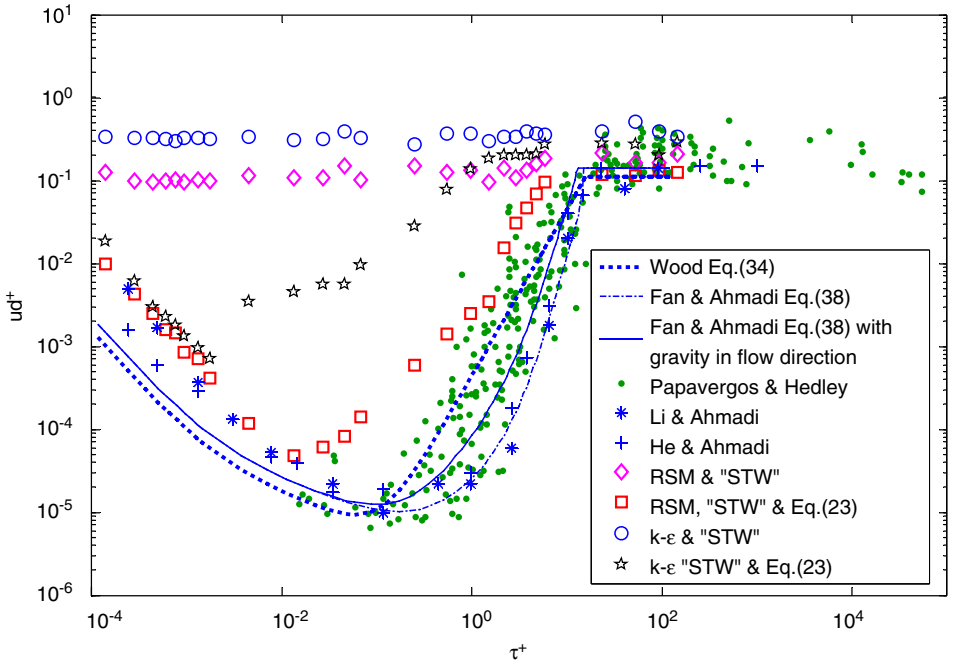

Fig. 7. Comparison of deposition velocity as predicted by the PARTICLE code (current simulation) and earlier results in a vertical duct with gravity in the flow direction.

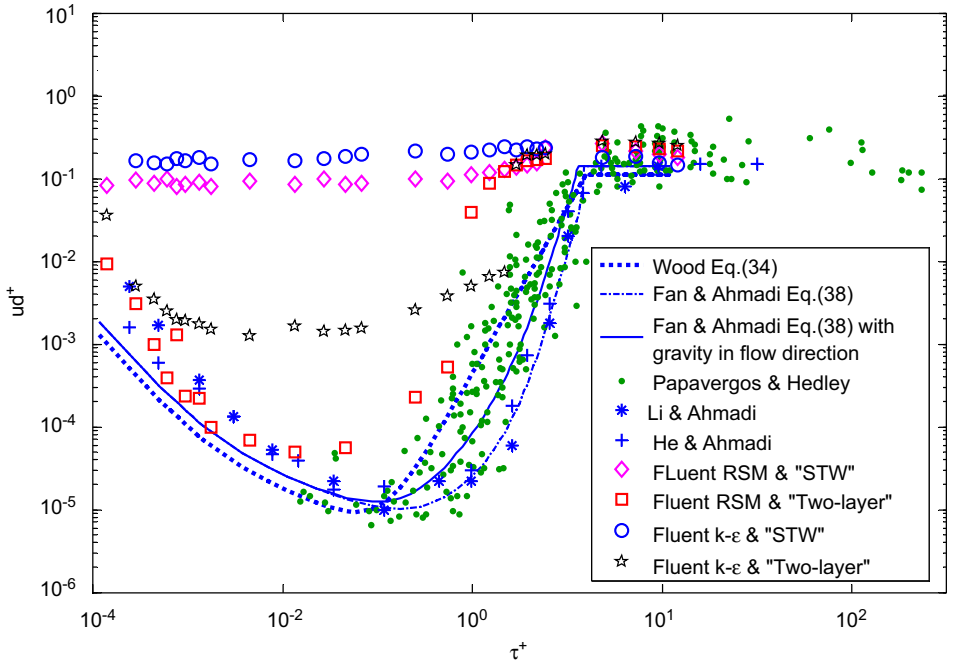

Fig. 8. Comparison of deposition velocity as predicted by the FLUENT^{TM} code (current simulation) and earlier results in a vertical duct with gravity in the flow direction.

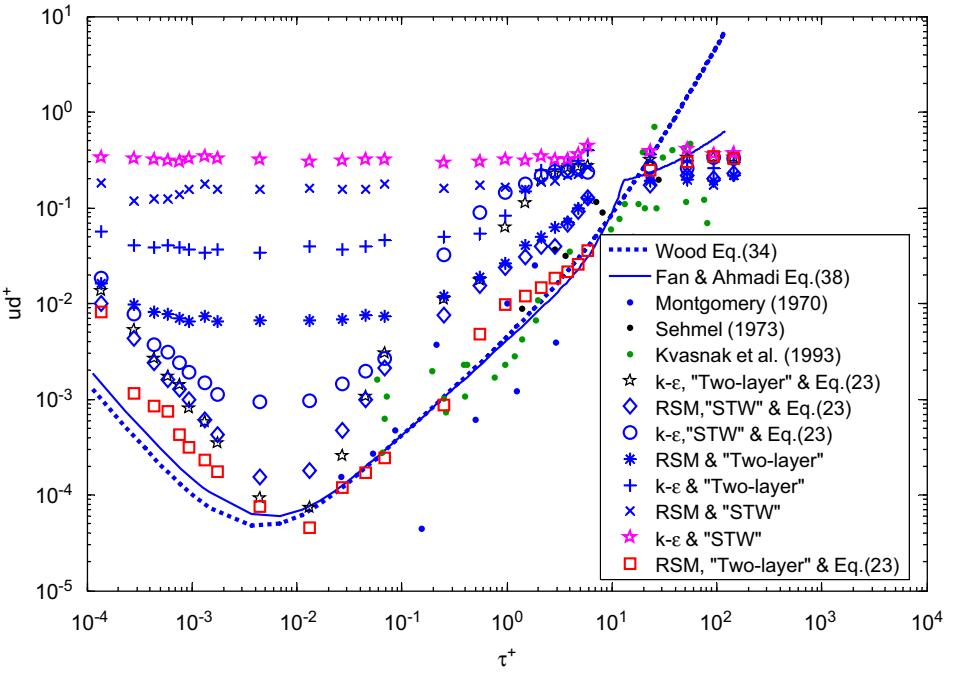

Fig. 9. Comparison of deposition velocity as predicted by the PARTICLE code (current simulation) and earlier results in a horizontal duct with gravity perpendicular to the flow direction.

prediction. This model provides reasonable results for the Brownian and the inertial regions, but overestimates in the deposition velocity in the "transition" region. For particles with nondimensional relaxation time less than 0.5, the simulation result is similar to the one obtained with PARTICLE code by using RSM turbulence model, "two-layer zonal" boundary condition and the turbulence near-wall normal fluctuation correction by Eq. (23). When the k–ε model with the "two-layer zonal" boundary condition is used, the predicated deposition velocity is higher than the experimental data and the semi-empirical model over the entire range of particle sizes. For both the RSM and the k–ε turbulence models, when the standard wall function boundary condition is used, FLUENT^{TM} code significantly overestimates the deposition rate over the entire particle sizes including the Brownian and the inertial ranges.

Comparing Figs. 6–8, it is seen that the deposition velocities predicated by PARTICLE and FLUENT^{TM} codes agree in trend. The k–ε turbulence model always leads to higher particle deposition rate compared to the RSM model under the same conditions. The turbulence normal fluctuation near wall significantly affects the predicted deposition rate. The overpredication of particle deposition rates is generally associated with the higher values of the turbulence fluctuation normal to the wall in the model. For successful predications of the particle deposition rate, it is important that the normal turbulence fluctuation be correctly modeled. One key component is to account for the quadratic variation of v' near the wall as given by Eqs. (22) and (23) (Li & Ahmadi, 1992, 1993; Ounis et al., 1993). The simulation results presented in Figs. 6–8 show that the use of the RSM turbulence model with the "two-layer zonal" boundary condition, and inclusion of the correction given by Eqs. (22) and (23) for the turbulence normal fluctuation leads to the most accurate predication of particle deposition over the entire size range covering "Brownian," "transition" and the "inertia region."

To study the deposition rate in a horizontal duct a series of computer simulations were performed and the results are presented in Figs. 9 and 10. Here both PARTICLE and FLUENT^{TM} codes were used and the accuracy of the turbulence model and the boundary conditions used are studied. It is assumed that the gravitational force is toward the lower wall that leads to additional deposition mechanism.

Fig. 9 shows the variation of the nondimensional particle deposition velocity, u_d^+, as a function of nondimensional particle relaxation time, τ^+ for different models and boundary conditions as predicted by PARTICLE code. The RSM and the k–ε turbulence model with the "two-layer zonal" boundary condition and/or the standard wall function boundary

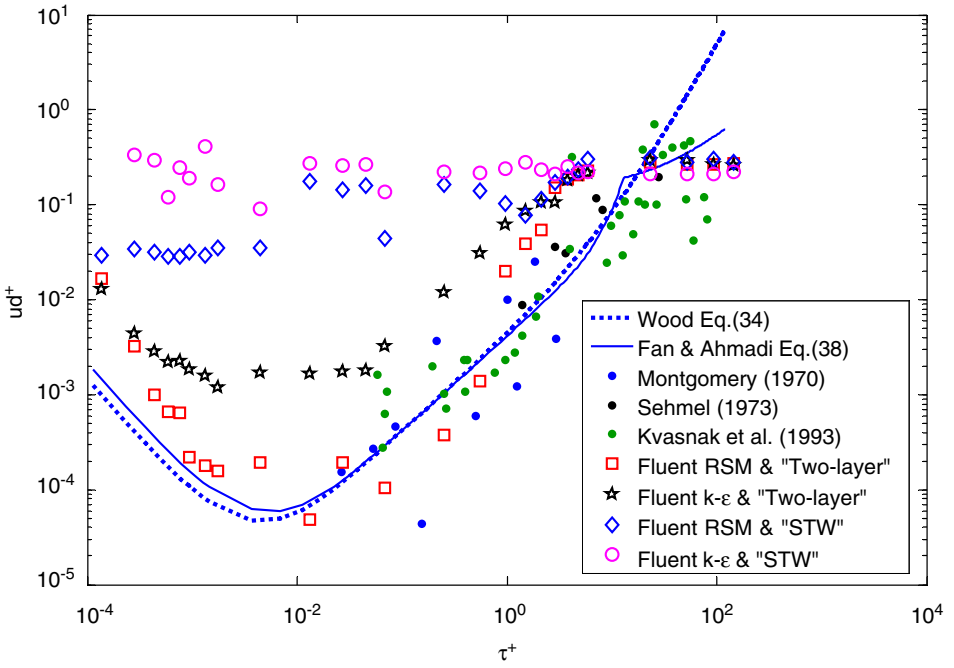

Fig. 10. Comparison of deposition velocity as predicated by the FLUENT^{TM} code (current simulation) and earlier results in a horizontal duct with gravity perpendicular to the flow direction.

condition were used in these analyses. For each case the effect of inclusion or omission of the near-wall correction given by Eqs. (22) and (23) is studied. The experimental data of Montgomery and Corn (1970), Sehmel (1973) and Kvasnak, Ahmadi, Bayer, and Gaynes (1993), and the empirical equations of Wood (1981), Fan and Ahmadi (1993) are plotted in this figure for comparison. The experimental data, the semi-empirical equations and simulations results presented in Fig. 9 show that the deposition velocities have a "V-shaped" variation similar to the case for the vertical duct. When compared to the "V-shaped" deposition curve of the vertical duct presented in Figs. 6 and 7, it is seen that the deposition velocity in the horizontal duct deposition is noticeably higher in the transition and the inertial regions. This is because the gravitational sedimentation increases the deposition velocity and becomes the leading deposition mechanism in the transition range. In the Brownian region, molecular diffusion is the dominant mechanism for particle deposition, and the deposition rate is not affected by the effect of gravity.

Fig. 9 shows that the RSM model with the "two-layer zonal" boundary condition and the near-wall "quadratic variations" correction given by Eqs. (22) and (23) leads to the deposition velocities that are closest to the experimental data and the semi-empirical models predictions. Similar to results for vertical duct shown in Figs. 6 and 7, Fig. 9 shows that the k–ε turbulence model always leads to higher deposition velocity when compared with the RSM model. For the highly refined mesh used, it is also seen that the standard wall function boundary condition leads to significant overestimation of the deposition rate even with the inclusion of the near-wall correction. It is also seen that the predicted deposition velocities by the RSM model in the latter half of the transition region (for 2 to 9 μm particles) are less sensitive to the correction for turbulent fluctuations. That is, the simulation results for different boundary conditions are not too far apart. This is because in the horizontal duct for the transition region particle sizes, the gravitational sedimentation becomes the dominant deposition mechanism. Therefore, the effect of model differences on particle deposition rate becomes less pronounced compared to the vertical duct. For the k–ε turbulence model the significant overpredication of the k–ε model still overwhelms the effect of gravitational sedimentation.

To study the accuracy of FLUENT^{TM} code for evaluating the particle deposition in horizontal ducts, a series of simulations identical to those presented in Fig. 9 were performed. However, the study of the effect of inclusion or omission of the near-wall normal fluctuation correction given by Eq. (23) was not included due to the unavailability

of the source code. The simulation results are presented in Fig. 10. It is seen that the RSM model with "two-layer zonal" boundary condition provides results that are reasonably close to the experimental data and the semi-empirical model predictions. This particularly is the case for particle smaller than 1 μm. The predication of the k–ε model with the "two-layer zonal" boundary condition, however, is higher than the experimental data and semi-empirical model prediction for the "Brownian" and the "transition" particle size ranges. For both the RSM and the k–ε turbulence models, when the standard wall function boundary condition is used, FLUENT^{TM} code significantly overestimates the particle deposition rates over entire size ranges.

6. Conclusions

In this study the accuracy of different computational models for predicting particle deposition in the turbulent duct flows was studied. Particular attention was given to the effect of using the "standard wall function," the "two-layer zonal" boundary conditions, and the importance of proper modeling of the near-wall turbulence fluctuations. Both FLUENT^{TM} code and PARTICLE (customized C++) code were used in the analysis. Instantaneous turbulent fluctuations were modeled with the continuous filtered white noise model (CFWN) and the discrete random walk model (DRW). The particle trajectory analysis was performed by PARTICLE code and the discrete phase module of FLUENT^{TM} code. On the basis of the presented results, the following conclusions are drawn:

- The RMS model, which accounts for the anisotropy of turbulence, provides a more accurate description of the turbulent flow field near wall. Accuracy of the flow field is critical for proper simulation of nano- and micro-particle depositions in turbulent flows.
- The k–ε turbulence model, which assumes isotropy, leads to high level of fluctuation perpendicular to the wall and to overpredication of nano- and micro-scale particle deposition rates.
- The CFWN and DRW turbulent fluctuation models are both effective stochastic methods for simulating instantaneous turbulent fluctuations for the particle deposition study.
- For high-resolution mesh, the "two-layer zonal" boundary condition is preferable and leads to more accurate prediction of turbulent flows and particle deposition rates. However, very close to the wall ($y^+ < 4$), the turbulence fluctuation velocities are still overpredicted. This could cause inaccuracy in the predicted particle deposition rates in the "Brownian" and "transition" regions as estimated by FLUENT^{TM} DPM module, and PARTICLE code.
- For high resolution mesh, the "standard wall function" boundary condition leads to rather large overprediction of the turbulent fluctuation velocity in the near-wall region as well as high level of particle deposition rate. The inaccuracy is more pronounced for the "Brownian" and the "transition" regions for particles in the size range of 0.01–8 μm.
- Accounting for the "quadratic variation of the turbulence near-wall fluctuations" as given by Eq. (23) is critical for accurate evaluation of the particle deposition rate. When used with the RSM turbulence model and the "two-layer zonal" boundary condition, this leads to most accurate evaluation of particle deposition rate among the various models studied.
- Turbulence diffusion significantly affects particle deposition rates in the "Brownian" and "transition" size regions. Thus, for accurate evaluation of the deposition rate, the turbulence fluctuations need to be properly modeled.
- The deposition rate of particle larger than 10 μm ("inertia region") is affected by the turbulence fluctuation level to a lesser extent and therefore is less sensitive to the modeling in accuracy.
- When the RSM turbulence model and the "two-layer zonal" boundary condition are used, the presented results indicate that FLUENT^{TM} code leads to reasonable prediction of the deposition rates of nano- and micro-particles (less than 1 μm). The predicated deposition velocities in vertical ducts for the "transition" size region, however, are higher than the experimental data. The k–ε turbulence model and the "standard wall function" boundary condition of FLUENT^{TM} code lead to significant overestimation of the deposition velocity.
- The most accurate predication of particle deposition rates is obtained by using the RSM turbulence model together with the "two-layer zonal" boundary condition, and use of PARTICLE code that included the correction for the near-wall quadratic variation of the turbulence normal fluctuations.

While the present study was focused on duct flows, the general conclusions in regard to the accuracy of various approximations are expected to be applicable to flows in complex passages of industrial interest.

Acknowledgments

The research is supported by the National Institute for Occupational Safety and Health (NOISH) and the Center for Air Resources Engineering and Science at Clarkson University.

References

Balashazy, I., & Hofmann, W. (1995). Deposition of aerosols in asymmetric airway bifurcations. *Journal of Aerosol Science*, *26*, 273–292.

Chen, H. C., & Patel, V. C. (1988). Near-wall turbulence models for complex flows including separation. *AIAA Journal*, *26*, 641–648.

Fan, F., & Ahmadi, G. (1993). A sublayer model for turbulent deposition of particles in vertical ducts with smooth and rough surfaces. *Journal of Aerosol Science*, *24*, 45–64.

FLUENT User's Guide (1998). Lebanon, NH: Fluent Inc.

Graham, D. I., & James, P. W. (1996). Turbulent dispersion of particles using eddy interaction models. *International Journal of Multiphase Flow*, *22*, 157–175.

He, C., & Ahmadi, G. (1999). Particle deposition in a nearly developed turbulent duct flow with electrophoresis. *Journal of Aerosol Science*, *30*, 739–758.

Hidy, G. M. (1984). *Aerosols, an industrial and environmental science*. New York: Academic Press.

Hinds, W. C. (1984). *Aerosol technology: Properties, behavior, and measurement of airborne Particles*. New York: Wiley.

Hinze, J. O. (1975). *Turbulence*. (2nd ed.), New York: McGraw-Hill.

Hutchinson, P., Hewitt, G. F., & Dukler, A. E. (1971). Deposition of liquid or solid dispersions from turbulent gas streams: A stochastic model. *Chemical Engineering Science*, *26*, 419–439.

Kallio, G. A., & Reeks, M. W. (1989). A numerical simulation of particle deposition in turbulent boundary layers. *International Journal of Multiphase Flow*, *15*, 433–446.

Kim, J., Moin, P., & Moser, R. D. (1987). Turbulent statistics in fully developed channel flow at low Reynolds number. *Journal of Fluids Mechanics*, *177*, 133–166.

Kvasnak, W., Ahmadi, G., & Schmidt, D. J. (2004). An engineering model for the fuel spray formation of deforming droplets. *Atomization and Sprays*, *14*, 289–339.

Kvasnak, W., Ahmadi, G., Bayer, R., & Gaynes, M. (1993). Experimental investigation of duct particle deposition in a turbulent channel flow. *Journal of Aerosol Science*, *24*, 795–815.

Lai, A. C. K., & Nazaroff, W. W. (2000). Modeling indoor particle deposition from turbulent flow onto smooth surfaces. *Journal of Aerosol Science*, *31*, 463–476.

Launder, B. E., Reece, G. J., & Rodi, W. (1975). Progress in the development of a Reynolds-stress turbulent closure. *Journal of Fluid Mechanics*, *68*(3), 537–566.

Launder, B. E., & Spalding, D. B. (1972). *Lectures in Mathematical Models of Turbulence*. London, England: Academic Press.

Li, A., & Ahmadi, G. (1992). Dispersion and deposition of spherical particles form point sources in a turbulent channel flow. *Aerosol Science and Technology*, *16*, 209–226.

Li, A., & Ahmadi, G. (1993). Deposition of aerosols on surfaces in a turbulent channel flow. *International Journal of Engineering Science*, *31*, 435–451.

Li, A., & Ahmadi, G. (1995). Computer simulation of particle deposition in upper tracheobronchial tree. *Aerosol Science and Technology*, *23*, 201–223.

Martonen, T. B., Zhang, Z., & Yang, Y. (1992). Interspecies modeling of inhaled particle deposition patterns. *Journal of Aerosol Science*, *23*, 389 –406.

Matida, E. A., Nishino, K., & Torii, K. (2000). Statistical simulation of particle deposition on the wall from turbulent dispersed pipe flow. *International Journal of Heat and Flow*, *21*, 389–402.

McLaughlin, J. B. (1989). Aerosol particle deposition in numerically simulated channel flow. *Physics of Fluids A*, *1*, 1211–1224.

Montgomery, T. L., & Corn, M. (1970). Aerosol particle deposition in a pipe with turbulent air flow. *Journal of Aerosol Science*, *1*, 185–213.

Oesterle, B., & Zaichik, L. I. (2004). On Lagrangian time scales and particle dispersion modeling in equilibrium turbulent shear flows. *Physics of Fluids*, *16*, 3374–3384.

Ounis, H., & Ahmadi, G. (1990). Analysis of dispersion of small spherical particles in a random velocity field. *Transactions of the ASME*, *112*, 114–120.

Ounis, H., Ahmadi, G., & McLaughlin, J. B. (1993). Brownian particle deposition in a directly simulated turbulent channel flow. *Physics of Fluids A*, *5*, 1427–1432.

Papavergos, P. G., & Hedley, A. B. (1984). Particle deposition behaviour from turbulence flows. *Chemical Engineering Research and Design*, *62*, 275–295.

Saffman, P. G. (1965). The lift on a small sphere in a slow shear flow. *Journal of Fluid Mechanics*, *22*, 385–400.

Schuen, J. S., Chen, L. D., & Faeth, G. M. (1983). Evaluation of a stochastic model of particle dispersion in a turbulent round jet. *A.I.Ch.E. Journal*, *29*(1), 167–170.

Thomson, D. J. (1987). Criteria for the selection of stochastic models of particle trajectories in turbulent flows. *Journal of Fluid Mechanics*, *180*, 529–556.

Uijttewaal, W. S. J., & Oliemans, R. V. A. (1996). Particle dispersion and deposition in direct numerical and large eddy simulations of vertical pipe flows. *Physics of Fluids*, *8*, 2590–2604.

Wang, Q., & Squires, K. D. (1996). Large eddy simulation of particle-laden turbulent channel flow. *Physics of Fluids*, *8*, 1207–1223.

Wang, Y., & James, P. W. (1999). On the effect of anisotropy on the turbulent dispersion and deposition of small particles. *International Journal of Multiphase Flow*, *25*, 551–558.

White, F. M. (2006). *Fluid Mechanics*. (6th ed.), New York: McGraw-Hill.

Wolfshtein, M. (1969). The velocity and temperature distribution in one-dimensional flow with turbulence augmentation and pressure gradient. *International Journal of Heat and Mass Transfer*, *12*, 301–318.

Wood, N. B. (1981). A simple method for the calculation of turbulent deposition to smooth and rough surfaces. *Journal of Aerosol Science*, *12*, 275–290.

Zhang, H., & Ahmadi, G. (2000). Aerosol particle transport and deposition in vertical and horizontal turbulent duct flows. *Journal of Fluid Mechanics*, *406*, 55–80.

Zhang, Z., & Kleinstreuer, C. (2001). Flow structure and particle transport in a triple bifurcation airway model. *Transaction of ASME*, *123*, 320–330.